International Journal of GEOMATE
(Geotechnique, Construction Materials and Environment)
ISSN: 2186-2982 (P), 2186-2990 (O), Japan
Vol. 31, Issue 145, September 2026, PP. 182-191; DOI: 10.21660/2026.145.g15300

EXCAVATION TESTS ON ALUMINUM ROD MODEL GROUND TO SIMULATE GROUND HEAVE

*Moe Yagawa[1], Hidetoshi Nishioka[2], Shinji Konishi[3] and Satoshi Sakata[4]

[1]Department of Civil, Human and Environmental Science and Engineering, Chuo University, Japan;
[2]Department of Civil and Environmental Engineering, Chuo University, Japan;
[3]Asano Taiseikiso Engineering Co., Ltd., Japan;
[4]Tokyo Metro Co., Ltd., Japan

*Corresponding Author, Received: 30 May 2026, Revised: 07 June 2026, Accepted: 10 June 2026

ABSTRACT: When performing the open-cut method, ground heave due to excavation may impact existing structures, causing deformation and other effects. Therefore, predicting the effects of ground heave near structures and considering countermeasures is essential. However, the interaction between the structure and ground during ground heave is not fully understood, leading to discrepancies between predictions and actual measurements. We analyzed this interaction through model experiments. Initially, we conducted an excavation experiment using an aluminum rod model ground that simulates sand behavior in two dimensions to assess whether ground heave could be accurately reproduced. This model enables image-based analysis to capture displacement and strain distribution near structures. We placed two earth retaining wall models, each 200 mm high, in a model ground measuring 1000 mm in width and 400 mm in height. Using a ground anchor model, we subjected the walls to tension equivalent to the earth pressure at rest. The primary experimental variable was the distance between the earth retaining walls. The intervening ground was excavated, and images were analyzed to assess the resulting ground behavior. Results confirmed that the aluminum rod model ground could simulate the upward vertical displacement patterns similar to those of the actual ground. These findings provide valuable reference data for future model experiments involving embedded structures such as tunnels.

Keywords: Ground heave, Aluminum rod model, Excavation test, Image analysis

1. INTRODUCTION

In urban areas, many cases have been reported in which nearby excavation induces ground settlement, heave, or lateral displacement, damaging nearby structures [1-3]. Excavation reduces overburden pressure, causing the release of in-situ stresses and resulting in upward deformation at the excavation base, a behavior known as ground heave [4]. When open-cut excavation occurs near existing underground structures, it is crucial to assess the impact of ground heave and accurately predict the resulting ground deformation. Accurate prediction requires an understanding of ground-structure interaction, and various analytical approaches have been proposed for this purpose [5-7]. Moreover, experimental data on this interaction during ground heave are still limited, and methods for predicting such deformation need further development. Consequently, discrepancies may still exist between predicted and observed ground deformation [8].

Previous studies have investigated the effects of excavation-induced ground deformation on adjacent tunnels using various approaches, including three-dimensional finite element method (3D-FEM) analysis and centrifuge model tests. For instance, a simplified prediction method has been proposed to evaluate the zone of influence on adjacent tunnel displacements caused by deep excavation in thick soft soil [7]. However, most of these studies focused primarily on lateral displacement or ground settlement. Experimental investigations on tunnels located directly beneath or adjacent to an excavation are limited, particularly with respect to their longitudinal bending deformation induced by ground heave (Fig. 1).

To experimentally investigate such deformation behavior, a model ground capable of reproducing excavation-induced stress release and allowing detailed observation of ground deformation is required. The aluminum rod model ground (Fig. 2) has been widely used in geotechnical model tests since the 1960s. For example, aluminum rod model grounds have been applied to studies of braced excavations [9] and tunnel excavations [10]. In addition, they have been used in various geotechnical problems, including shallow foundations, retaining structures, and underground excavations [11–15].

Owing to its nonlinear stress–strain relationship and dilatancy characteristics, the aluminum rod model ground can be regarded as a two-dimensional model of medium-dense sand [16,17]. Furthermore, because the internal deformation of the ground can be directly observed from the side surface, image analysis techniques can be employed to evaluate displacement and strain distributions within the ground [18]. These features make the model particularly suitable for investigating excavation-induced ground deformation and soil–structure interaction. In addition, its simplicity and high reproducibility enable systematic parametric investigations under various experimental conditions.

However, the fundamental ground heave behavior and unloading characteristics of the model ground itself have not been sufficiently clarified. Therefore, this study investigates the ground heave characteristics of the aluminum rod model ground through excavation tests. In addition, biaxial extension tests were conducted to examine its fundamental unloading characteristics.

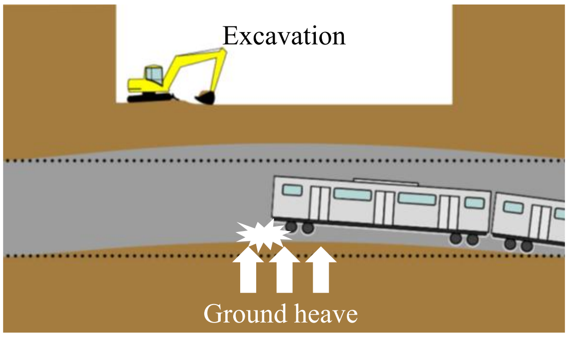

Fig. 1 Influence of excavation on an existing subway tunnel

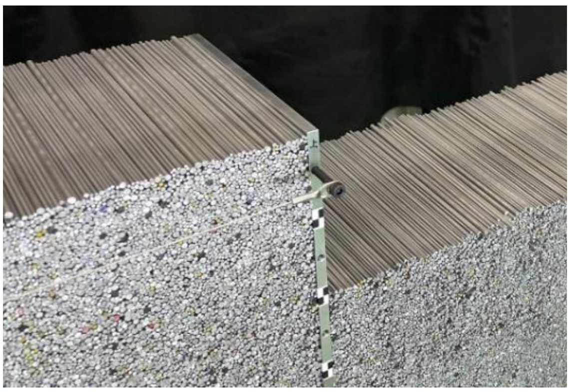

Fig. 2 Aluminum rods

The remainder of this paper is organized as follows. Section 2 describes the research significance of this study. Section 3 reports the summary of the excavation experiment using the aluminum rod model ground. Section 4 presents the experimental results, including the displacement distribution obtained through image analysis. Finally, the conclusions of this study are summarized. Additionally, the results of the biaxial extension test on the aluminum rods are provided in the Appendix.

2. RESEARCH SIGNIFICANCE

No previous studies have simulated ground heave using an aluminum rod model. This experiment enhances our understanding of the ground heave characteristics of the aluminum rod model. The data provide fundamental insights for future excavation experiments near existing structures and into the mechanical behavior of the aluminum rod model ground under unloading conditions. Future experiments will improve the prediction accuracy of ground heave and develop more reliable evaluation methods for the effects on existing underground structures.

3. EXPERIMENT SUMMARY

3.1 Model Ground

Fig. 2 depicts the aluminum rod model ground, and Fig. 3 illustrates the experimental apparatus used in this study. The model ground was prepared using three types of aluminum rods with diameters of 1.5 mm, 2 mm, and 3 mm in equal weight proportions (1:1:1). The overall dimensions of the model ground were 1000 mm in width and 400 mm in height. Preparation involved placing 50 mm-thick layers of aluminum rods and compacting each layer using a small vibrator. The unit weight was 21.5 kN/m^3.

When the model ground reached a height of 200 mm (half the total height), a level ensured the surface was parallel to the base. Cross markers were placed at 30 mm intervals (Fig. 4) for image analysis. These markers were cross-pattern blocks affixed to a wooden board (1 mm thick, 7 mm wide, and 160 mm long). Two aluminum retaining wall models (6 mm thick, 200 mm high, and 150 mm deep) were installed vertically, with the distance between them (excavation width, *W*) either 400 mm or 250 mm (positions 300 mm or 375 mm from both ends of the model ground). The remaining 200 mm height was prepared using the same compaction method.

As illustrated in Fig. 5, a wire simulating a ground anchor was connected to the top and bottom ends of each retaining wall. Weights equivalent to the at rest earth pressure were attached to the wire ends.

Since retaining wall deformation was not the focus of this study, the at rest earth pressure (with $K_0 = 0.5$) was used to minimize experimental variation. These weights were suspended via pulleys to apply tensile force externally to the apparatus.

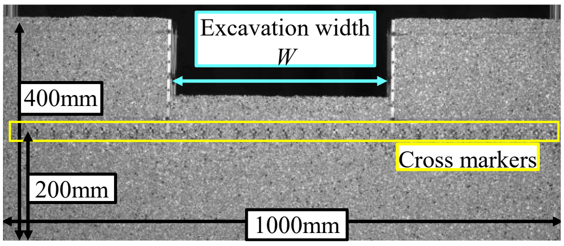

(a) Overall

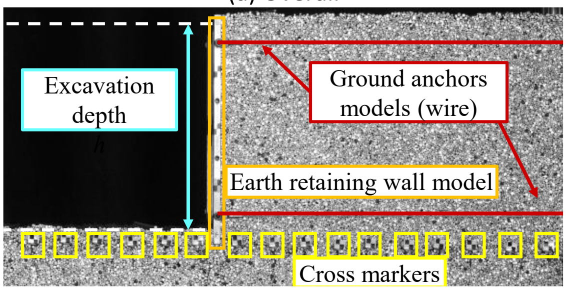

(b) Around the earth retaining wall on the right side

Fig. 3 Experimental apparatus

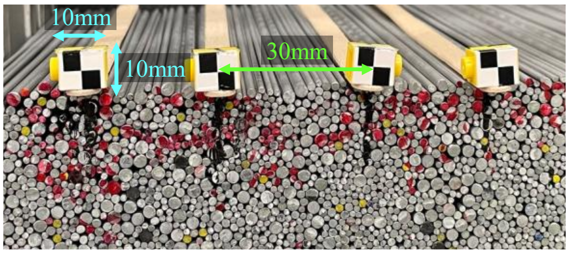

Fig. 4 Cross markers

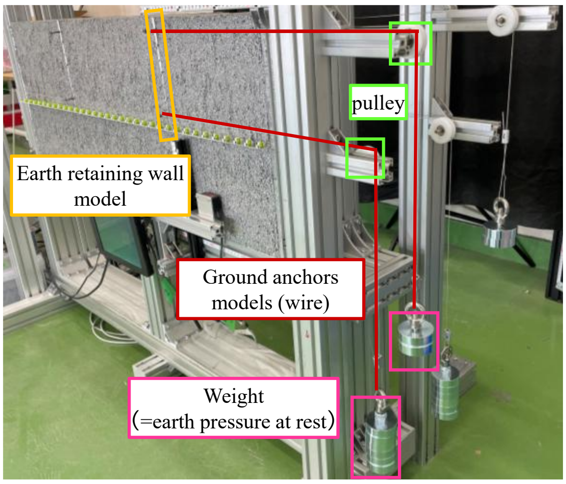

Fig. 5 Attached wires and weights

3.2 Testing Methods

Excavation of the ground model was performed as shown in Fig. 6. Excavation was conducted in incremental stages, with the thickness of each stage decreasing progressively as the excavation depth increased. A laser level projected the target depth for each excavation stage, guiding the placement of the aluminum rods from the front to the back of the model (Fig. 7). After each excavation, the weight of the excavated aluminum rods was measured and photographed using a digital camera (6000 × 4000 pixels, 0.2 mm/pixel) for image analysis. This process was repeated until the excavation depth h reached 190 mm, leaving a 10 mm overburden above the cross markers. Each test was replicated three times for excavation widths W of 400 mm and 250 mm, respectively.

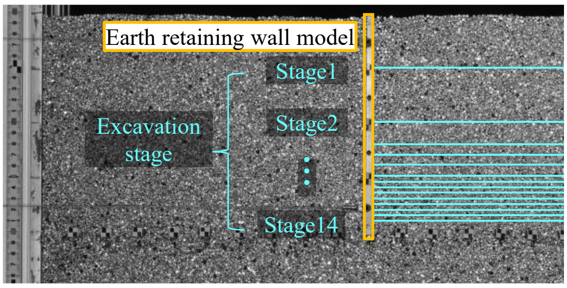

Fig. 6 Excavation stages

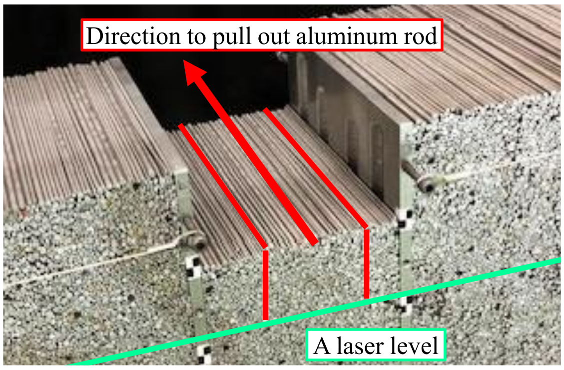

Fig. 7 Excavation of aluminum rods

4. EXPERIMENTAL RESULTS

4.1 Displacement Distribution Of Model Ground

Image analysis (Digital Image Correlation method with Ditect's DippStrain software) was used to obtain the vertical and horizontal displacement distribution at the excavation depth h = 190 mm (after excavation was completed). The results are presented in Figs. 8-11.

Fig. 8 and Fig. 9 show displacement distributions within ±1.0 mm. Fig. 8(a) and Fig. 9(a) illustrate significant vertical displacements concentrated in a narrow zone inside the retaining walls confirming ground heave in the model ground. Fig. 8(b) and Fig. 9(b) depict the horizontal displacements of the ground behind the retaining walls in the active pressure direction.

Fig. 10 and Fig. 11 present detailed displacement distributions within a narrower range of ±0.2 mm. These figures reveal upward vertical displacement occurring approximately 100 mm below the excavation bottom within the retaining walls, along with horizontal displacements toward the center of the model. Similar distribution results were obtained, regardless of *W*.

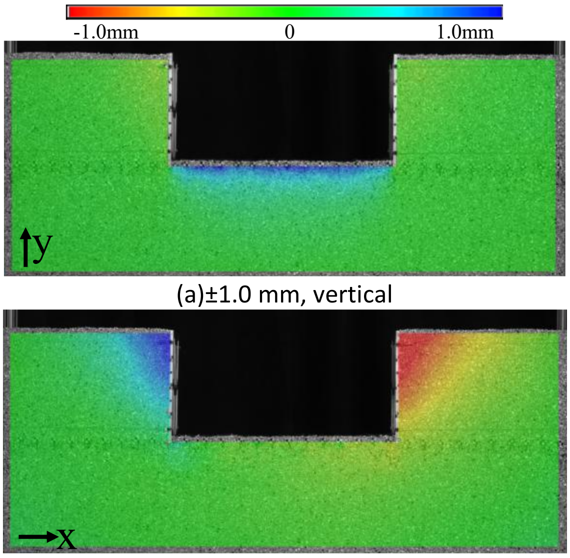

(a)±1.0 mm, vertical

(b) ±1.0 mm, horizontal

Fig. 8 Displacement distribution (*W* = 400 mm)

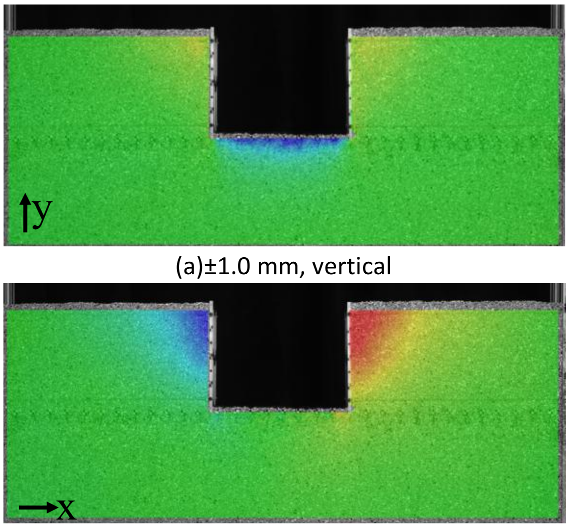

(a)±1.0 mm, vertical

(b) ±1.0 mm, horizontal

Fig. 9 Displacement distribution (*W* = 250 mm)

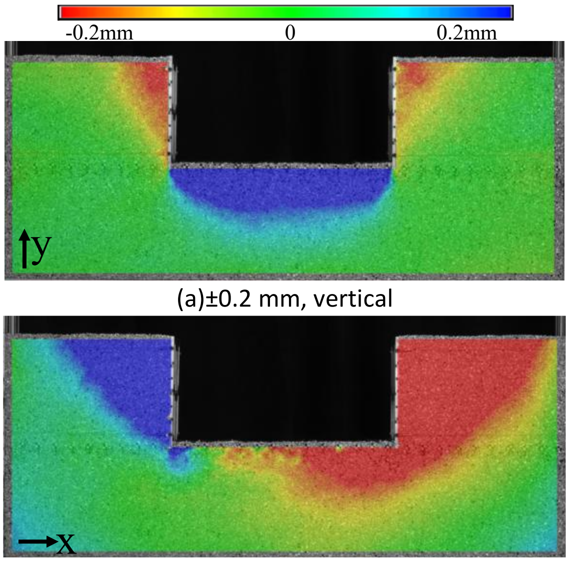

(a)±0.2 mm, vertical

(b) ±0.2 mm, horizontal

Fig. 10 Displacement distribution (*W* = 400 mm)

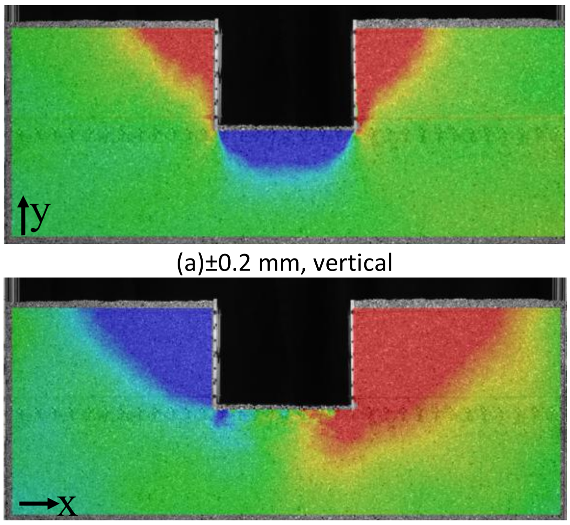

(a)±0.2 mm, vertical

(b) ±0.2 mm, horizontal

Fig. 11 Displacement distribution (*W* = 250 mm)

4.2 Vertical Displacement Of Each Cross Marker

The distribution of vertical displacement, defined as ground heave displacement δ_g, was analyzed at each cross marker, which was initially placed under an overburden of 200 mm. The vertical displacement at the excavation depth h = 190 mm (end of excavation), corresponding to the reduction of overburden from 200 mm to 10 mm, was calculated using the correlation tracking function of Ditect's Dipp-Motion V software. Note that this method generally provides sub-pixel accuracy; that is, the measurement error is less than 1 pixel (0.2 mm) in this study. The relationship between δ_g and the distance from the model center is shown in Fig. 12(a) for W = 400 mm and in Fig. 12(b) for W = 250 mm.

The cross markers, located ±200 mm (W = 400 mm) or ±125 mm (W = 250 mm) from the model center, were positioned beneath the retaining wall. As the retaining walls settled during excavation, δ_g in these locations became negative.

In contrast, within the excavation area, the distribution of δ_g appears approximately rectangular, when averaged, as indicated by the orange lines in Fig. 12. This rectangular distribution shape aligns with the ground displacement predictions from 3D finite element analysis in a previous study [19].

Although the heave displacement at the excavation bottom was not uniform, variations were observed among individual cross markers. Each experiment focused on cross markers within the retaining walls—12 points for W = 400 mm and 6 points for W = 250 mm—excluding any markers located less than 30 mm from the retaining walls. Box plots illustrating the range of δ_g variations are shown in Fig. 12. Across the three experiments, the averaged values were δ_g = 0.87 mm and 0.90 mm for

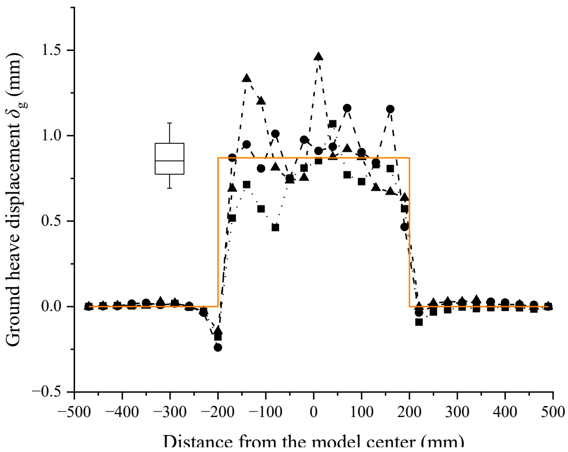

(a) W = 400 mm

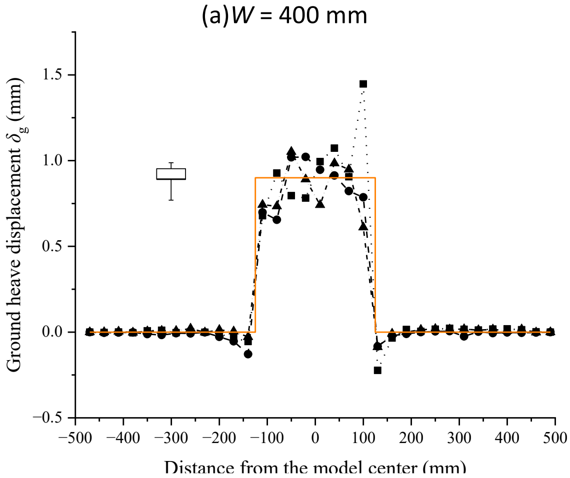

(b) W = 250 mm

Fig. 12 Horizontal distribution of ground heave displacement

W = 400 mm and 250 mm, respectively. The standard deviations were 0.11 mm and 0.07 mm.

These variations were clearly larger than those observed outside the excavation area and therefore cannot be attributed solely to the accuracy of image analysis. Because the overburden thickness was extremely small—only 10 mm—at the final stage of excavation, it is likely that manual excavation caused slight local movements of the cross markers. However, these fluctuations can be regarded as occurring randomly among the three tests, and it is evident that averaging the results provides a nearly constant displacement within the excavation area.

4.3 Change In Ground Heave With Progress Of Excavation

The value of δ_g at each excavation stage was obtained by averaging the displacements of the cross markers within the excavation area. Fig. 13 presents these averaged values of δ_g. The lower horizontal axis of Fig. 13 shows the excavation rate, calculated by dividing the excavation depth h by the initial overburden thickness (200 mm), while the corresponding overburden pressure is indicated on the upper horizontal axis. The average axial strain of the lower ground, calculated by dividing δ_g (shown on the left vertical axis) by the height of the ground below its measurement position (200 mm), is shown on the right vertical axis.

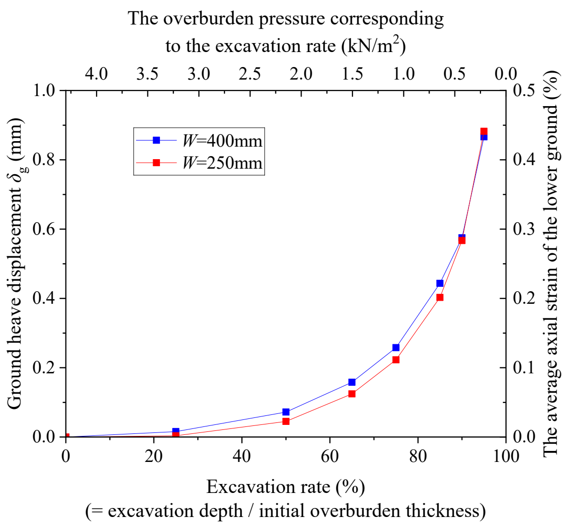

Fig. 13 Variation in ground heave displacement according to the stage of excavation

By considering the heave of the model ground as an increase in axial strain caused by unloading, the unloading behavior of the model ground was observed to be nonlinear, as shown in Fig. 13. This nonlinear stress–strain tendency agrees reasonably well with the results of the biaxial extension (unloading) test presented in the Appendix, supporting the validity of this interpretation. In addition, the aluminum rod model ground clearly exhibits ground heave and, moreover, allows such deformation to be captured easily through image analysis. These advantages suggest that this model ground has potential applicability for investigating the interaction between ground heave and tunnel deformation during excavation.

4.4 Comparison Of Previous Studies And The Results Of This Experiment

To compare the ground heave behavior observed in this study with that of actual sandy ground, results from centrifuge excavation tests on Toyoura sand [20] were used for comparison. Fig. 14 presents the centrifuge model used in the Toyoura sand excavation tests [20]. The L6 measurement point at the center of the excavated area in Test S was selected for comparison because no tunnel existed beneath the excavation. The model ground was prepared using Toyoura sand, achieving an average dry density of 1546 kg/m³, corresponding to a relative density D_r of 69%. The centrifuge acceleration was set to 60 g. Within the diaphragm walls, $ZnCl_2$ fluid—density adjusted to match Toyoura sand—was placed inside the latex membranes, and excavation was simulated by draining the fluid in three stages. The model ground consisted of dry sand, so the influence of groundwater was not considered. The vertical displacement at the excavation center in Test S was extracted for each stage. A plot of ground heave displacement versus excavation rate was prepared, as shown in Fig. 15.

A comparison of Figs. 13 and 15 indicates that the average maximum heave for the aluminum rod ground is 0.88 mm (corresponding to 0.44% average axial strain in the lower ground), whereas for Toyoura sand, it is 0.17 mm (corresponding to 0.028% average axial strain). Additionally, the ground heave of Toyoura sand due to unloading occurs almost linearly, in contrast to the nonlinear heave observed in the aluminum rod model.

As aluminum rods are an artificial material distinct from natural sand, it is unsurprising that the quantitative relationship between excavation rate and strain shown in Fig. 13 does not match that of Toyoura sand in Fig. 15. Nevertheless, the aluminum rod model ground exhibited a clear monotonic increase in strain during excavation, sufficiently distinct to be detected through image analysis. Although the aluminum rods are fundamentally two-dimensional elements and have idealized circular cross sections, in contrast to the three-dimensional irregular particles of natural soil, the mechanism by which this simple assembly reproduces such qualitative ground behavior remains unclear. Even so, the ability of the aluminum rod model ground to reproduce excavation-induced heave provides a useful new insight for modeling ground–tunnel interaction.

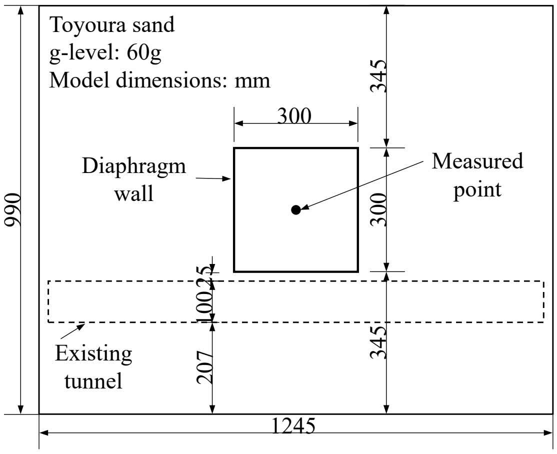

(a) Plan view

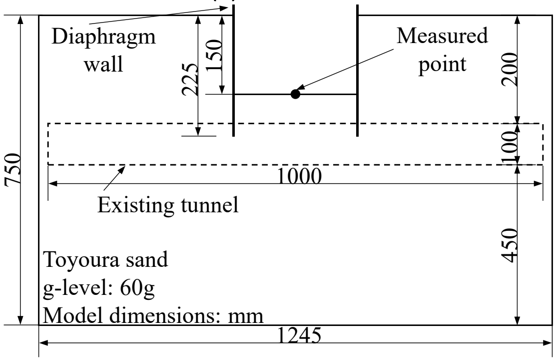

(b) Elevation view

Fig. 14 Centrifuge model setup [20]

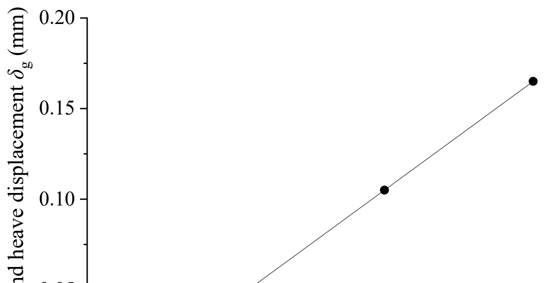

Fig. 15 Variation in ground heave displacement with excavation progress

5. CONCLUSION

In this study, excavation tests utilized an aluminum rod model. We confirmed that ground heave can be simulated by combining image analysis with excavation tests on a model ground. Regardless of excavation width, the average distribution shape of the excavation bottom was rectangular, aligning with previous studies. The change in ground heave with excavation progress was confirmed to be nonlinear.

The results provide reference data for future excavation experiments. Future work will focus on subway tunnels, using the same experimental model to embed a model of an existing tunnel in the longitudinal direction. Excavation over this model will simulate nearby excavation work. The primary experimental parameters will include excavation width *W* and tunnel model bending stiffness *EI*. We will investigate the influence of these factors on the vertical displacement of the tunnel caused by ground heave.

6. ACKNOWLEDGMENTS

We would like to thank Editage (www.editage.jp) for its English language editing services.

7. APPENDIX: BIAXIAL EXTENSION TEST ON ALUMINUM RODS

A.1 Experimental Overview

To investigate the unloading behavior of the aluminum rod model ground, a biaxial extension test (corresponding to a triaxial extension test on sand after K_0-consolidation) was conducted as an element test. In this test, the vertical stress (σ_v) was decreased while maintaining a constant horizontal stress (σ_h) on the specimen mixed with aluminum rods. Notably, the "extension" in this test does not involve applying direct tensile force to the specimen, instead, the extension state was produced solely by reducing the vertical stress σ_v from the initial K_0-consolidated condition.

Fig. A-1 shows a schematic front view of the biaxial testing apparatus, while Fig. A-2 presents a photograph of the apparatus. The testing procedure is outlined as follows.

A specimen of the aluminum rod model ground was prepared with the same mixing ratio as in the excavation test. The specimen size was 200 mm × 200 mm and 150 mm deep, with a unit weight of 21.6 kN/m^3. The sidewalls were fixed during preparation, and an initial vertical stress (σ_{v0}) was applied via the loading plate. The applied stress was 4.35 kN/m², which corresponds to the initial overburden pressure in the excavation test. The initial vertical stress (σ_{v0}) was applied not by the jack but by the self-weight of the loading plate and an additional weighting plate placed between the plate and the jack.

The side confinement plates compressed the specimen laterally through wire tension. The wire attached to the left confinement plate passed in front of and behind the aluminum rods, routed through a pulley on the right side, and connected to the weighting plate. This mechanism applied a constant horizontal stress (σ_h) to the specimen throughout the test.

To simulate the K_0-consolidation condition, the reduced stress calculated from K_0 = 0.5 was used as

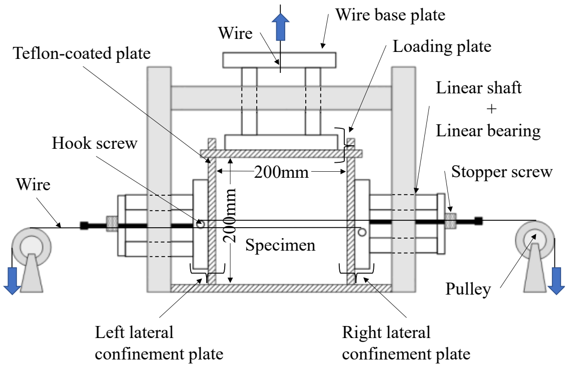

Fig. A-1 Schematic view of the biaxial testing apparatus

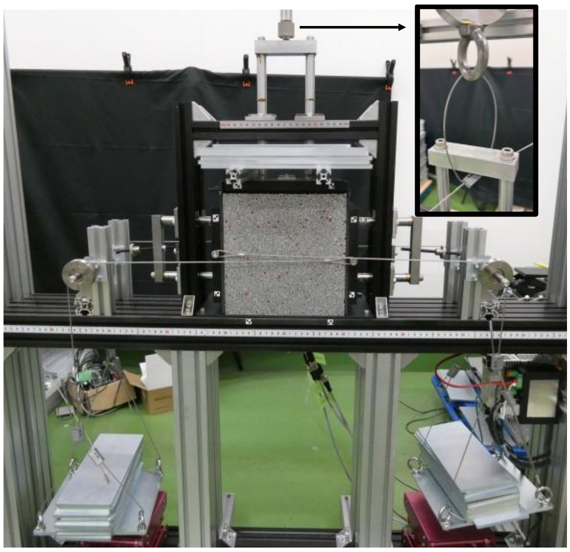

Fig. A-2 Photograph of the biaxial testing apparatus the weight of the weighting plate (2.17 kN/m^2), which applied the corresponding horizontal pressure through the side confinement plates. After this setup, the sidewall fixation was released.

The loading plate was connected to an electric displacement-controlled jack via a wire, and unloading was applied upward. The decrease in vertical load was measured using a load cell attached directly to the jack. The vertical stress (σ_v) was calculated by dividing the measured load by the initial top surface area of the specimen. In contrast, the horizontal stress (σ_h) was obtained by dividing the weight of the weighting plate by the initial side surface area.

Displacements of the loading plate and both side confinement plates were calculated using image analysis (correlation tracking function of Ditect's Dipp-Motion V software, 0.11 mm/pixel), as in the excavation test. The unloading rate was set to 0.01 mm/s, and the test continued until the separation of the loading plate from the specimen surface was visually confirmed.

A.2 Experimental Results

Fig. A-3 shows the tracked marker positions obtained from the image analysis and the tracking results at the end of the test. The tracking markers were placed approximately 7 mm inward from each edge, with five markers assigned along each side. The displacement of each marker was obtained by performing pattern matching within a 70-pixel × 70-pixel window centered on the marker.

The vertical strain ε_v was calculated from the difference between the average vertical positions of the five markers along the top and bottom edges of the specimen. The corresponding vertical strain ε_v and the vertical stress σ_v were obtained at each step within this range. Vertical stress σ_v was determined from the jack load displayed on the monitor captured images.

Fig. A-4 illustrates the relationship between the vertical stress σ_v and vertical strain ε_v. No distinct peak is observed in the stress–strain relationship.

In the horizontal direction, almost no displacement was observed, indicating that the mechanism behind this behavior requires further investigation. One possible explanation is that the sidewalls hardly moved due to frictional resistance, which may have resulted in a non-uniform horizontal stress σ_h distribution within the specimen. Although these factors may influence deformation behavior in the biaxial extension test, a more detailed analysis requires additional tests under varied conditions. Thus, further investigation is required in future work.

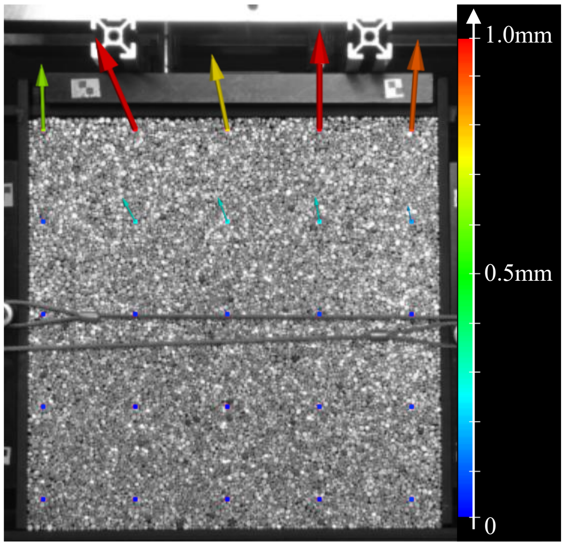

Fig. A-3 Trajectories of tracking markers in image analysis

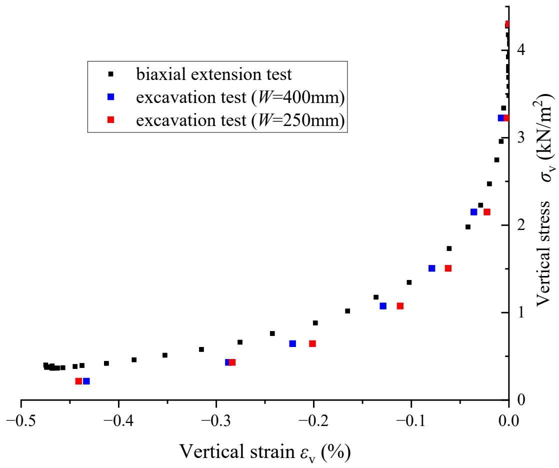

Fig. A-4 Relationship between vertical stress σ_v and vertical strain ε_v

A.3 Relationship to Displacement Observed In Excavation Tests

Using the same procedure as in the excavation test (Figs. 8–11), the displacement distribution was obtained and is shown in Fig. A-5. Both tests exhibited similar vertical displacement patterns. However, in the biaxial extension test, deformation was non-uniform throughout the specimen; only the upper approximately 100 mm of the specimen displayed deformation.

Additionally, Fig. A-4 compares the relationship between vertical strain ε_v and released overburden pressure σ_v from both the excavation and biaxial extension tests.

The two tests demonstrate a comparable trend in overall deformation response, indicating that the biaxial extension test effectively reproduces the vertical deformation behavior observed during excavation.

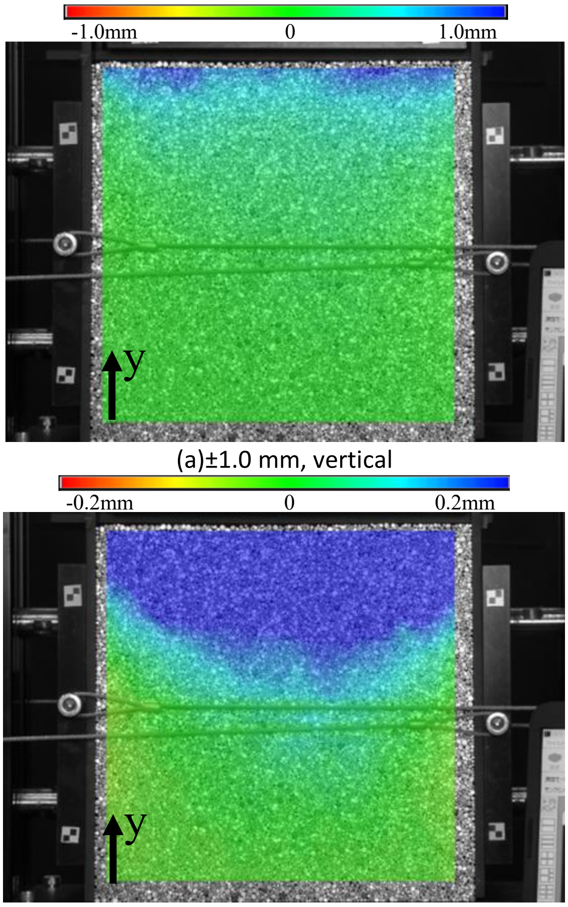

(a)±1.0 mm, vertical

(b) ±0.2 mm, vertical

Fig. A-5 Displacement distribution

8. REFERENCES

1. Korff M., Deformations and damage to buildings adjacent to deep excavations in soft soils, Delft University of Technology / Deltares, 2009. https://resolver.tudelft.nl/uuid:bb4d9200-9fab-4333-a0d9-7fd9b24e1b71
2. Endicott L.J., Design and construction of excavations in an urban setting–Lessons learnt from failures, In International Conference on Geotechnical Engineering - ICGE Colombo, 2015, pp. 57-66.
3. Nguyen H.N., Effects of the construction of deep foundation pits by the open excavation method on the deformation of neighboring houses, GEOMATE Journal, Vol. 27, No. 120, 2024, pp. 17-26. https://doi.org/10.21660/2024.120.4382
4. Japanese Geotechnical Society, Technical terms for geotechnical engineering, Maruzen Publishing, Japan, 2006, p. 331 (in Japanese).
5. Zhussupbekov A., Omarov A., and Tanyrbergenova G., Design of anchored diaphragm wall for deep excavation, GEOMATE Journal, Vol. 16 No. 58, 2019, pp. 139-144. https://doi.org/10.21660/2019.58.8240
6. Teparaksa W., Deep basement excavation in soft Bangkok clay closed to places, GEOMATE Journal, Vol. 12 No. 33, 2017, pp. 85-90. http://dx.doi.org/10.21660/2017.33.2622
7. Liu B., Shao C.M., Wang N.N., and Zhang D.W., Influenced zone of deep excavation and a simplified prediction method for adjacent tunnel displacement in thick soft soil, Applied Science, Vol.13, No.7, 2023, 4647. https://doi.org/10.3390/app13074647
8. Sakata S., Nishioka H., Yagawa M., and Konishi S., Prediction and analysis of the impact of ground rebound caused by nearby open-cut construction on subway structures in the longitudinal direction and its construction, 31st Proceedings of Jointed Railway Technology, No. 24-45, 2024 (in Japanese). https://doi.org/10.1299/jsmetld.2024.33.SS4-2-4
9. Nakai T., Kawano H., Murata K., Banno M., and Hashimoto T., Model tests and numerical simulation of braced excavation in sandy ground: Influences of construction history, wall friction, wall stiffness, strut position and strut stiffness, Soils and Foundations, Vol.39, No.3, 1999, pp.1-12. https://doi.org/10.3208/sandf.39.3_1
10. Shahin H.M., Nakai T., Hinokio M., Kurimoto T., and Sada T., Influence of surface loads and construction sequence on ground response due to tunneling, Soils and Foundations, Vol.44, No.2, 2004, pp.71-84. https://doi.org/10.3208/sandf.44.2_71
11. Nanasato S., Nishino F., Nishioka H., and Shimada T., FE analysis of the influence of sliding on the seismic strain transfer ratio between the ground and cut and cover tunnels in contact with bearing stratum, Japanese Geotechnical Society Special Publication, Vol. 10, No. 20, 2024, pp. 736-740. https://doi.org/10.3208/jgssp.v10.OS-9-06
12. Kikuchi A., Nishioka H., Kato Y., Nasu A., Okamoto M., and Nagatani H., Model tests on the effects

of head fixation and separation distance double sheet pile earth retaining wall method, the 3rd International Conference on Press-in Engineering, 2024, pp. 526-532.

13. Shikakura R., Nishioka H., Yamakuri Y., Arai T., and Hirano M., Experimental study on the effect of penetration length and eccentricity of sheet pile foundation on bearing capacity, the 3rd International Conference on Press-in Engineering, 2024, pp. 533-539.
14. Sagawa T., Ohata T., and Nishioka H., 2D model tests of sheet pile reinforcement method for existing pile foundations, Climate Change Adaptation from Geotechnical Perspectives, Springer, 2024, pp. 105-114. https://doi.org/10.1007/978-981-99-9215-7_10
15. Sasaki Y., and Nishioka H., Vertical loading tests on local scoured spread foundation on aluminum rods model ground, GEOMATE Journal, Vol. 23, No. 98, 2022, pp. 17-23. https://doi.org/10.21660/2022.98.1472
16. Hirakawa D., Tanimoto S., Watanabe K., Takahashi H., Nishioka H., and Ito K., Technique of the preparation for the model ground of physical model test in geotechnics, Geotechnical Engineering Magazine, Vol. 71, No. 11, 2023, pp. 46-59 (in Japanese).
17. Kikumoto M., Nakai T., Zhang F., and Shahin H., Two dimensional model tests using aluminum rods mass, Geotechnical engineering magazine, Vol. 56, No. 10, 2008, pp. 12-15 (in Japanese). https://ndlsearch.ndl.go.jp/books/R000000004-I9671395
18. Osakabe T., Kouda M., Sato H., Ishii M., Tamura M., Matsuzawa K., and Kumada T., Model experiments for earthquake-resistant performance of geotextile using aluminum rod layer, Proceedings of the 4th Asian Regional Conference on Geosynthetics, Vol. 4, No. E.11.08, 2006, pp.1515-1518.
19. Okada H., Nakamura M., Kasai Y., Kurihara M., and Yamamoto M., Prediction for behavior of ground heave and existing tunnel due to open cut, Proceedings of the Japan Society of Civil Engineers, Vol. 2004, No. 763, 2004, pp. 53-69 (in Japanese). https://doi.org/10.2208/jscej.2004.763_53
20. Ng C.W.W., Shi J., and Hong Y., Three-dimensional centrifuge modelling of basement excavation effects on an existing tunnel in dry sand, Canadian Geotechnical Journal, Vol. 50, No. 8, 2013, pp. 874-888. https://doi.org/10.1139/cgj-2012-0423